Elucidating the Sources of Activity and Stability of FeP Electrocatalyst for Hydrogen Evolution Reactions in Acidic and Alkaline Media

Xin Zhao,[a] Zheng Zhang,[b] Xun Cao,[a] Jun Hu,[c,*] Xinghua Wu,[a,d] Andrew Yun Ru Ng,[e] Guo-Ping Lu,[f] Zhong Chen[a,*]

a School of Materials Science and Engineering, Nanyang Technological University, 50 Nanyang Avenue, Singapore 639798, Singapore
b Institute of Materials Research and Engineering, A*STAR (Agency for Science, Technology and Research), #08-03, 2 Fusionopolis Way, Innovis, Singapore 138634, Singapore
c School of Chemical Engineering, Northwest University, Xi'an 710069, P. R. China
d School of Materials & Energy, Guangdong University of Technology, Guangzhou 510006, Guangdong, P. R. China
e Division of Chemistry and Biological Chemistry, School of Physical and Mathematical Sciences, Nanyang Technological University, 21 Nanyang Link, Singapore 637371.
f School of Chemical Engineering, Nanjing University of Science & Technology, Xiaolingwei 200, Nanjing 210094, P. R. China.

E-mail: hujun32456@163.com, ASZChen@ntu.edu.sg

Abstract

In this study, we conduct comprehensive experimental and theoretical investigations on the hydrogen evolution reaction (HER) preformation of FeP electrode in acidic and alkaline solutions. Theoretically, bulk Fe-O bond is unfavorable, but surface Fe-O bond is favorable and plays a negative role for HER. The presence of oxygen bonds (native or formed during reaction) is the root source of the reduced HER activity. Surface treatment in 37% HCl solution removes the oxide layer and significantly improves the HER performance, especially in alkaline solution. After etching, the overpotentials in 0.5M H_2SO_4 are 79 and 95 mV at 10 and 20 mA cm^{-2}, respectively. The ones in 1M KOH are 95 and 102 mV at 10 and 20 mA cm^{-2}, respectively. Long-term instability in alkaline solution is caused by the presence of oxygen in the electrolyte. Good stability can be realized by removing oxygen from the solution.

Key words: Hydrogen evolution reaction; Iron phosphides; Nanosheet structure; Stability; DFT calculations

1. Introduction

Hydrogen is a promising clean and renewable energy source to solve the problem of fossil fuel depletion and the increasing environmental issue. Electrolysis of water to produce hydrogen has attracted great amount of attention in recent years, particularly with the development of the solar cells to generate renewable electricity.[1-6] Pt-based materials exhibit high efficiency as cathode catalysts for hydrogen evolution reaction (HER) by water reduction. However, the scarcity and high cost limit its application.

Recently, transition metal dichalcogenides, carbides, borides, nitrides, phosphides have emerged as promising candidates for the HER due to their advantages such as earth-abundance and high activity.[7-10] Among them, transition metal phosphides have been very attractive due to their low cost, robust stability, and high catalytic activity in acidic environment.[11-13] Given that Fe is the second abundant metal on Earth's crust, Fe-based phosphide materials are promising as HER catalysts for practical applications. Toward this effort, Xu et al. have reported FeP nanosheets as an HER catalyst in acidic electrolyte, but the reported FeP has a large overpotential of ~240 mV at 10 mA cm^{-2}.[14] Sun et al. improved the activity by growing FeP nanowire on conductive Ti foil as an integrated 3D HER cathode, which showed exceptionally high activity with an overpotential of 55 mV at 10 mA cm^{-2}.[1] Afterwards, many other nanowire-type works were reported, including carbon cloth supported FeP nanowires,[15] porous FeP nanowire arrays on graphene sheets or carbon nanotubes composite materials,[16-18] FeP nanorods synthesized using anodized aluminum oxide template,[19] ZnO template assisted growth of FeP nanotubes.[20] Other forms include FeP nanoparticles grown on carbon cloth or graphene sheets,[21, 22] hollow microspheres assembled by nanosheet FeP, and the rugae-like FeP nanocrystal assembly on a carbon cloth.[23, 24] Besides morphology control, doping was also reported to improve the HER performance, such as Ni doping.[25, 26] In addition, Yu and coauthors reported that FeP/Ni_2P hybrid supported on 3D Ni foam had an excellent HER and OER activities, comparable or even better than commercial Pt and IrO_2 catalysts.[27] However, degradation in performance was noticed by many early works, and there has been a lack of understanding of the fundamental reasons among the diversified catalytic activities by different reports. It is noted that all these reports indicated the presence of Fe-O or P-O bond on the surface by XPS. However, little is known on whether and how these O bonds would affect the activity and stability. Hence, comprehensive experimental and theoretical studies of FeP are essential to better understand this material.

Aside from the activity, durability is also crucial to the practical application. Most of the reported results show that FeP is a stable HER catalyst in acidic media.[1] However, Park et al. found the current dropped with time in FeP nanowire arrays. They found that FeP arrays were more stable in base than in acid solution.[11] This is possibly due to the dissolution of Fe foil substrate in acid solution, which makes the results dubious on the true stability of FeP in acidic and alkaline solutions. So far, little has been reported on its stability in basic media. Luo et al. reported the activity of FeP nanowire arrays in 1 M KOH, the overpotential of which was 218 mV at 10 mA cm^{-2}.[15] However, they have not reported any stability data in this alkaline environment. Wang et al. and Feng et al. reported good durability of FeP in both acidic and basic electrolytes,[20, 28] while Park et al. and Wang et al. found a current drop with time in FeP.[11, 29] Therefore, it is necessary to comprehensively investigate the durability of FeP in both acidic and basic media, especially the latter that has not been thoroughly studied so far.

In this work, nanosheet-structured FeP catalyst grown on Ti foil was synthesized. The surface oxidation was carefully studied for its effect on the HER activity and stability using combined experimental and theoretical approaches. A solution to improve the activity and stability in the basic media has been suggested based on the understanding of the root cause for the degraded performance.

2. Experimental Section

2.1 Materials and synthesis: Ti foils, $(NH_4)_2Fe(SO_4)_2$ and CH_3COOK were purchased from Sigma Aldrich. H_2SO_4 was purchased from Honeywell and NaH_2PO_2 was purchased from Aladdin Ltd. (Shanghai, China). FeOOH films were synthesized by electrodeposition method according to previous reported work.[30] FeOOH films were electrodeposited on Ti foils using a configured glass cell at 70°C containing 0.01 M $(NH_4)_2Fe(SO_4)_2$ and 0.04 M CH_3COOK aqueous solution, in which a Ti foil (2 cm × 1 cm) was employed as the working electrode, a platinum foil as the counter electrode, and a Ag/AgCl electrode as a reference electrode. The voltage applied for electrodepositions was at 0.65 V vs. Ag/AgCl. The immersed area of the Ti foil was 1 cm^2. The duration of the deposition was set at 15 min. After the electrodeposition, the FeOOH films were washed thoroughly with DI water. To prepare FeP/Ti films, the electrodeposited FeOOH/Ti films and 0.5 g NaH_2PO_2 were placed at two separate positions in a porcelain boat with NaH_2PO_2 at the upstream side of the tube furnace. Before heating, the tube was vacuumed to -0.1 MPa and filled with Ar gas. The purging procedure was repeated for 3 times. Subsequently, the samples were heated at 400°C for 2 h with a heating rate of 2 °C/min in Ar atmosphere with the flow rate of 10 sccm. To optimize the performance, treatments at 300, 400, and 500°C were compared. The results showed that the best performance was obtained at 400°C. The amount of FeP on Ti foil was around 0.8 mg/cm^2. For comparison, commercial 20%Pt/C was employed to fabricate electrode on Ti foil for HER according to a previous report.[31] 10 mg of 20% Pt/C powder was dispersed in 1 mL of solution containing 0.95 mL of ethanol and 50 mL of 0.5 wt% Nafion. Then the mixture was ultrasonicated for 30 min. Pt/C solution was dropped onto the surface of the Ti foil for several times and then dried overnight. The amount of Pt/C was about 4 mg cm^{-2}.

2.2 Electrochemical measurements: All electrochemical measurements were conducted using CHI 660D potentiostat (CH Instruments, Inc.) in an H-type electrochemical cell with a proton exchange membrane (Nafion) between to separate the anode and cathode. The electrochemical cell is configured with a three-electrode system, with the FeP/Ti as the working electrode, a platinum foil as the counter electrode and a Ag/AgCl electrode as the reference electrode. The measured potentials vs. Ag/AgCl were converted to a reversible hydrogen electrode (RHE) scale according to the Nernst equation: $V_{RHE} = V_{Ag/AgCl} + 0.059pH + 0.197$. Linear sweep voltammetry (LSV) measurements were conducted in electrolyte with scan rate of 5 mV/s. 0.5 M H_2SO_4 and 1 M KOH aqueous solution were used as the electrolyte. In this work, only LSVs and Tafel plots were iR-corrected. The iR correction was taken as $V_{corrected} = V_{uncorrected} - jR$, where j is the current density (A cm^{-2}), R is the ohmic drop measured by the impedance spectroscopy.

2.3 Faradaic efficiency: The volume of H_2 generated was measured using water displacement method. The measurement was conducted using a sealed H-type electrochemical cell with a proton exchange membrane (Nafion) in between to separate the anode and cathode. The gas was collected through the hole on the Teflon cap of the cell via a Teflon tube to a measuring cylinder of 10 mL filled with water, which was immersed in the glass crystallizing dish upside down. H_2 yield was calculated by measurement of the gas volume in the headspace of the measuring cylinder through $V_{H_2} = nRT/p$, where $V_{H_2}(m^3)$ is the volume of H_2, n (mol) is the amount of H_2, R (8.3144598 J mol^{-1} K^{-1}) is the idea gas constant, T (K) is the temperature (294 K for room temperature during

the experiment in the lab), p (Pa) is the pressure of H_2. The amount of H_2 n is determined by $n = Q/(2eN_A)$, where Q (C) is the cumulative charge, e (1.6021892×10^{-19} C) is the electric charge of one single electron, N_A (6.02214086×10^{23} mol^{-1}) is the Avogadro constant.

2.4 Theoretical calculation: The CASTEP module of the Materials Studio software (Accelrys Inc.) was used for the theoretical calculations. The parameter setting follows the same as our previous calculation.[3] More details are available in the supporting information.

2.5 Characterization: The FeP/Ti thin films were characterized using field emission scanning electron microscopy (FESEM, JEOL JSM-7600F). Crystallinity was identified by X-ray diffraction (XRD, Shimadzu 6000 X-ray diffractometer) with Cu Kα radiation (λ = 0.154 nm). The chemical state of FeP/Ti was investigated by X-ray photoelectron spectroscopy (XPS, Thermo Fisher Scientific Theta Probe system). High-resolution transmission electron microscopy (HR-TEM) of the samples was characterized using a field-emission transmission electron microscope (FE-TEM, JEM-2100 F, JEOL, Japan). The elemental composition was determined by energy dispersive X-ray spectroscopy (EDS) using the genesis microanalysis system (EDAX) attached to the TEM.

3. Results and discussion

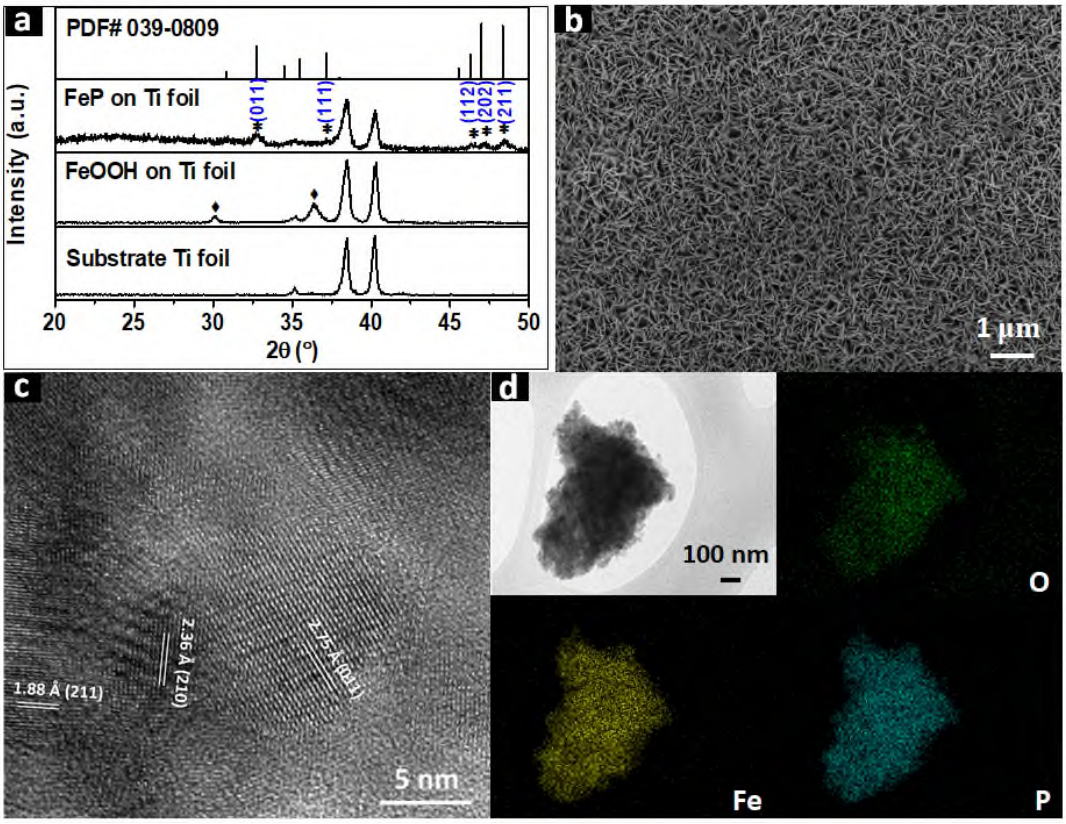

Figure 1. (a) XRD patterns and (b) SEM images of FeP/Ti. (c) A high-resolution TEM image of FeP. (d) EDS elemental mapping of O, Fe and P.

FeP/Ti was successfully synthesized by phosphidation of FeOOH/Ti using NaH_2PO_2 as the P source. Figure 1a shows the X-ray diffraction (XRD) pattern of the FeOOH/Ti by electro-deposition and phosphide after the phosphidation at 400 °C. Five peaks corresponding to the (011), (111), (112), (202), and (211) planes of FeP phase (PDF no. 039-0839) were observed. There is no impurity phase; the 3 peaks (around 35°, 38° and 40°) are from the substrate Ti foil. The as-synthesized FeP is black in color and exhibits nanosheet structure (Figure 1b). The nanosheet structure was observed in the prepared FeOOH before the phosphidation treatment (Figure S2), which means that phosphidation is a mild process. Figures 1c shows the transmission electron microscopy (TEM) image for FeP nanosheets. The high-resolution TEM image reveals a well-resolved lattice fringe and facets of (211), (210), (011) are observed. The EDS elemental mapping images confirm the uniform distribution of Fe and P (Figure 1d), and the ratio of Fe:P is very close to 1:1 (Table S1, Figure S3). In addition, O is also detected by EDS.

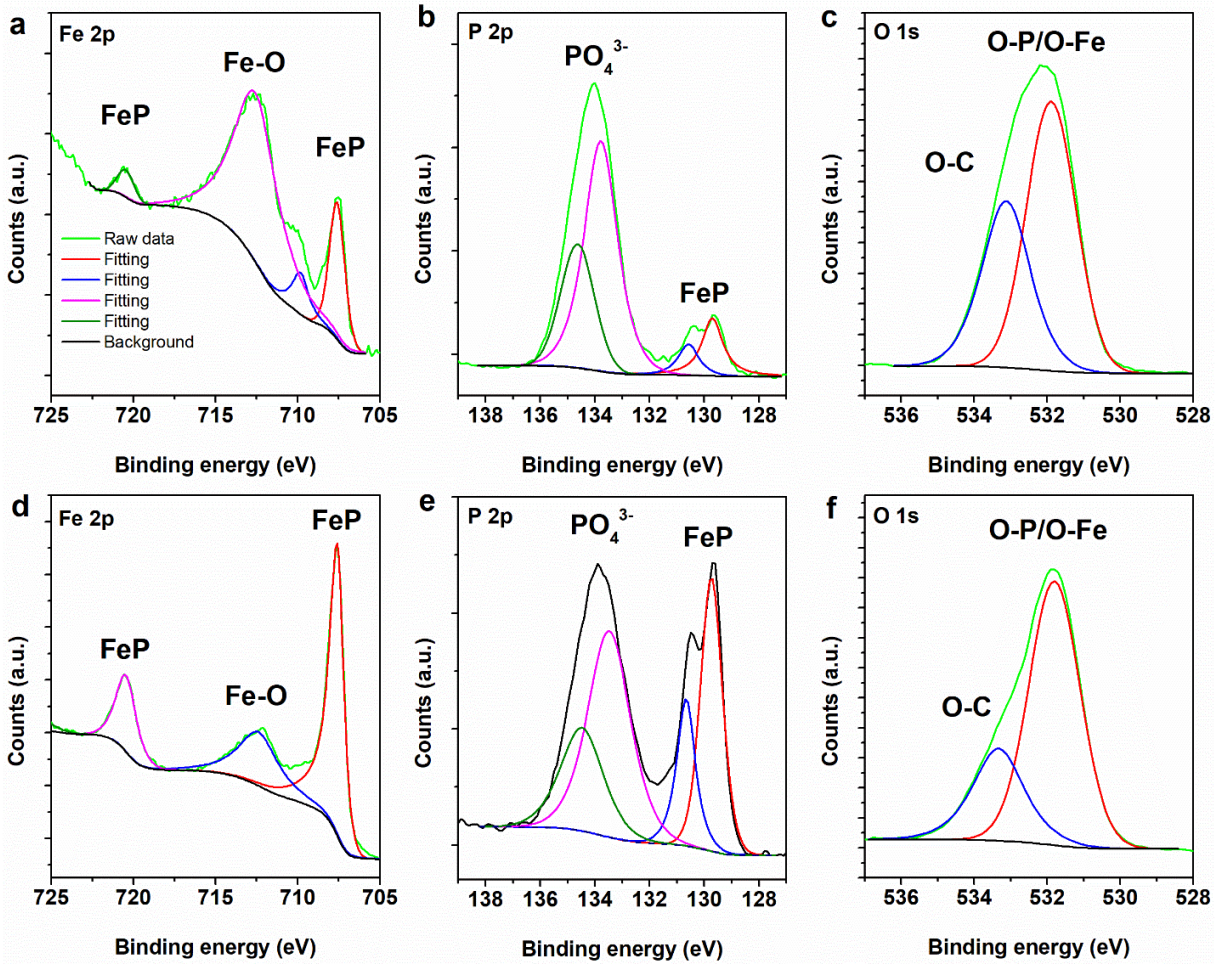

Figure 2. XPS spectra of Fe 2p, P 2p, and O 1s for FeP with phosphidation at 400°C before (a, b, c) and after (d, e, f) etching using HCl.

The surface chemical states of the as-synthesized FeP was analyzed by XPS (Figure 2a-c). In the Fe 2p core level spectra of as-synthesized FeP, the set of sharp peaks was observed at a lower

binding energy, represented by a 707.6 eV (Fe $2p_{3/2}$)/720.6 eV (Fe $2p_{1/2}$) doublet, and could be ascribed to FeP. This is in good agreement with previous reports.[20, 23] The Fe $2p_{3/2}$ peaks at 709.8 and 712.6 eV were observed, which were attributed to Fe^{3+} of Fe-O. Usually Fe^{3+} of iron oxides have satellite peaks, but they were not observed in the Figure 1a. Thus, we attribute the surface oxides to iron phosphate, which is consistent with the reported XPS of iron phosphate.[32] The P 2p core level spectra regions centered at lower binding energies of 129.7 eV ($2p_{3/2}$) and 130.3 eV (P $2p_{1/2}$) can be assigned to P-Fe in FeP, whereas the broad peak at higher binding energies can be ascribed to phosphate.[23] O 1s signal shows a broad peak that can be split into two peaks. The higher energy peak centered at 533.1 eV is ascribed to O-C bond arising from the absorbed carbon contamination on the surface. The one at lower binding energy can be assigned to O-P and O-Fe bond. The XPS analysis indicates that Fe-O and P-O bonds exist on the surface, which is possibly from iron phosphate.[32] The Fe-O and P-O species were also observed in the reported results of as prepared FeP.[16, 18] Thus, the oxides seem to be native and inevitable. In order to clarify whether the oxide layer can be avoided during synthesis, other phosphidation temperatures have been conducted under 300 and 500°C. It turns out that native oxide layer is inevitable in the as-synthesized FeP (Figure S4, and Table S2). And 400°C is favorable to form more FeP. Consistently, the best HER performance was achieved at the synthesis temperature of 400°C (Figure S5). Thus, it is concluded that surface native oxides have significantly negative impact on the HER performance. Moreover, it is confirmed that the HER performance and the oxygen content is strongly correlated. In the current analysis, we take the ratio of P-O and P-Fe content based on XPS measurement to represent the relative oxygen content. The amount of oxygen follows the order of 400°C < 500°C < 300°C (Table S3), which is consistent with the HER activity. Although the surface oxide is inevitable, it can be removed by acid etching. After the FeP/Ti electrode was soaked in HCl (37%) solution for 60s and washed with DI water, more FeP is exposed and the iron phosphate is mostly removed by etching as evidenced by XPS (Figure 2d-f). The XRD results also indicate that HCl treatment does not change the phase structure (Figure S6).

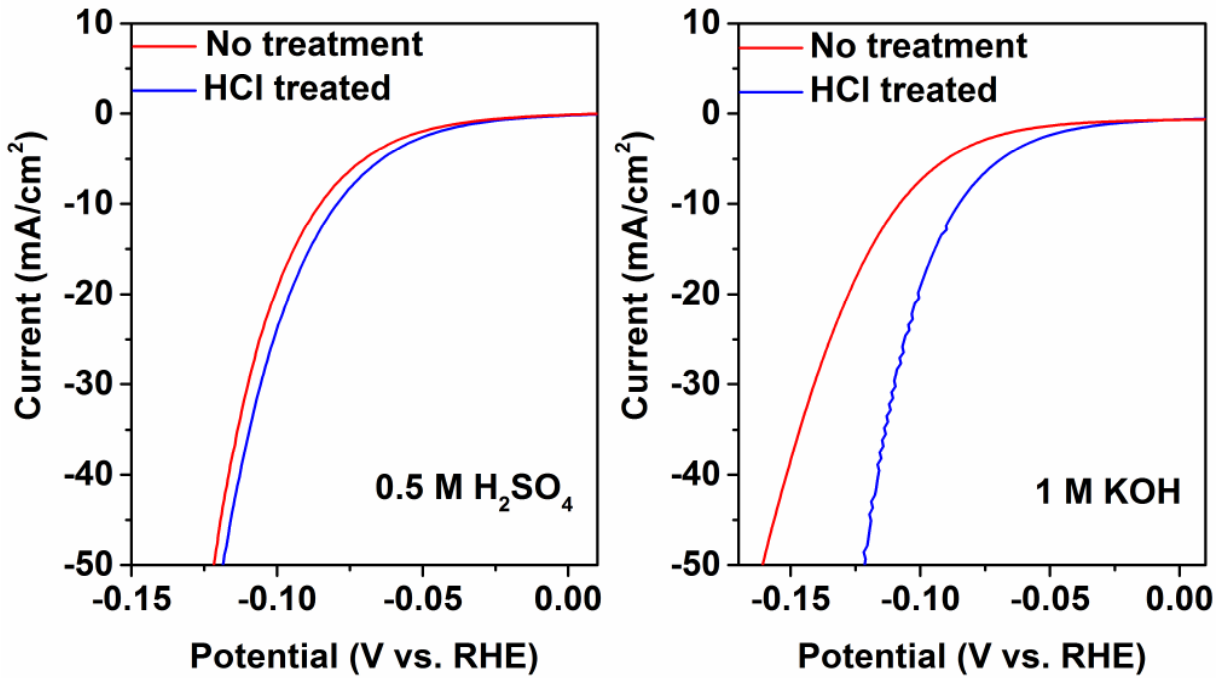

Figure 3. The comparison of HER performance in acid and alkaline of FeP treated with HCl (37%) for 60s.

The polarization curve with iR compensation (Figure S7, Table S4) is given in Figure 3 before and after HCl etching to investigate how the surface oxides affect the HER activity. The HER performance was improved compared with the one without surface treatment, especially in alkaline environment (Figure 3). After etching, the overpotentials in acidic electrolyte were 79 and 95 mV at 10 and 20 mA cm^{-2}, while in alkaline environment overpotentials were 95 and 102 mV at 10 and 20 mA cm^{-2}, respectively. The overpotentials in acid are comparable to the reported values of this material.[1, 20, 33, 34] Moreover, it is the first time to report such a low overpotential for HER using FeP in alkaline electrolyte after etching (Table S5) without any doping or surface modification. The HCl etching may also increase the number of surface sites, which leads to a higher HER performance. Thus, the electrochemical active surface areas (ECSA) of the FeP before and after the HCl etching have been measured. The results show that the ECSA after HCl etching decreases after etching (Figure S8), which indicates that the enhancement in HER activity after etching does not come from ECSA increase. Further investigation shows that HCl etching also works on all samples with different heat treatment temperatures (Figure S9).

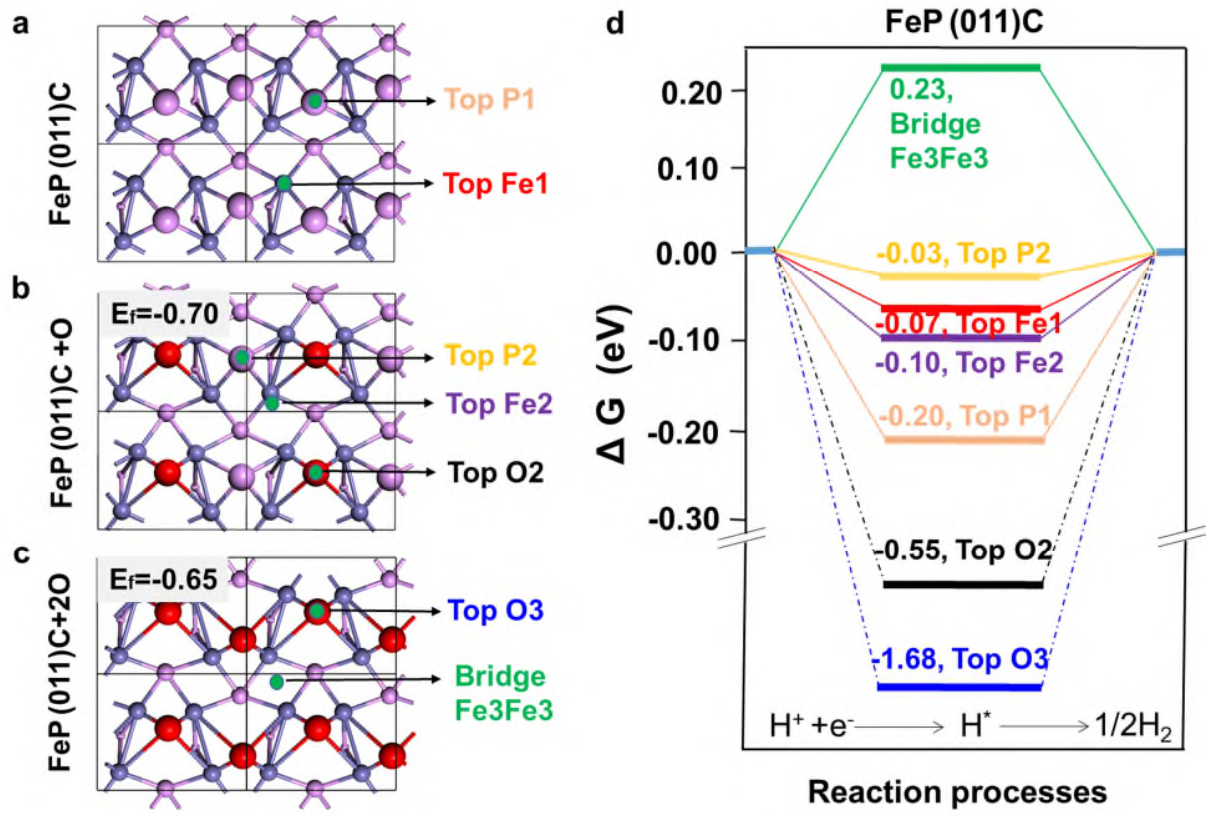

Figure 4. (a) Top view of replacing sites and reaction sites on (011)C surface for calculation of Gibbs free energies. (b) Top view of half P atoms replaced by O atoms and possible reaction sites for H_2 generation. The replacing formation energy (E_f) is -0.70 eV. (c) Top view of all P atoms replaced by O atoms and possible reaction sites for H_2 generation. The E_f is -0.65 eV. Violet spheres stand for P atoms, blue spheres stand for Fe atoms, red spheres stand for O atoms and green spheres stand for the adsorption sites of H atoms. (d) Gibbs free energies profile of H_2 generation on surface P and Fe sites on (011)C facets after replacing P atoms with O atoms.

Another issue that should not be ignored is the possibility of O replacing P atom in the lattice structure of FeP. We first investigated the formation energy of O replacing P atoms in the bulk FeP. Our theoretical calculation indicates it is not energetically favorable to replace P by O in the bulk FeP (Figure S10). Then the surface O replacing P was investigated. We use the (011) for the investigation, because the (011) surface has the lowest surface energy (Figure S11). There is one P site and one Fe site on the (011) surface for reaction (Figure 4a). The negative formation energy of replacing P with O atoms indicates that P atoms can be replaced by O atoms on the surface (Figure 4b and 4c). Thus, evaluation of how surface lattice O bond affects the HER performance was then conducted by theoretical calculation (Figure 4d). The HER activity of Top P2 is better after one P is replaced by O atom compared with Top P1 site on the clean surface without O atoms, while the activity of Top Fe1 becomes lower after O replacing P. If all possible P atoms are replaced by O atoms, the HER activity is very poor, because there are no active P sites, and Fe sites become less active. We also investigated another 2 facets (112) and (211) to check the effect of O replacement on the P site and Fe site activity. As shown in Figure S12, the HER activity is slightly decreased for Top P sites (free energy increase to 0.05 eV from 0.02 eV), but the free

energy for hydrogen evolution is still very small which indicates a good HER activity. However, O replacement has significantly reduced the HER activity on Fe site. Thus, it is concluded that O bonds on the surface will negatively affect the HER activity on Fe sites compared with P sites.

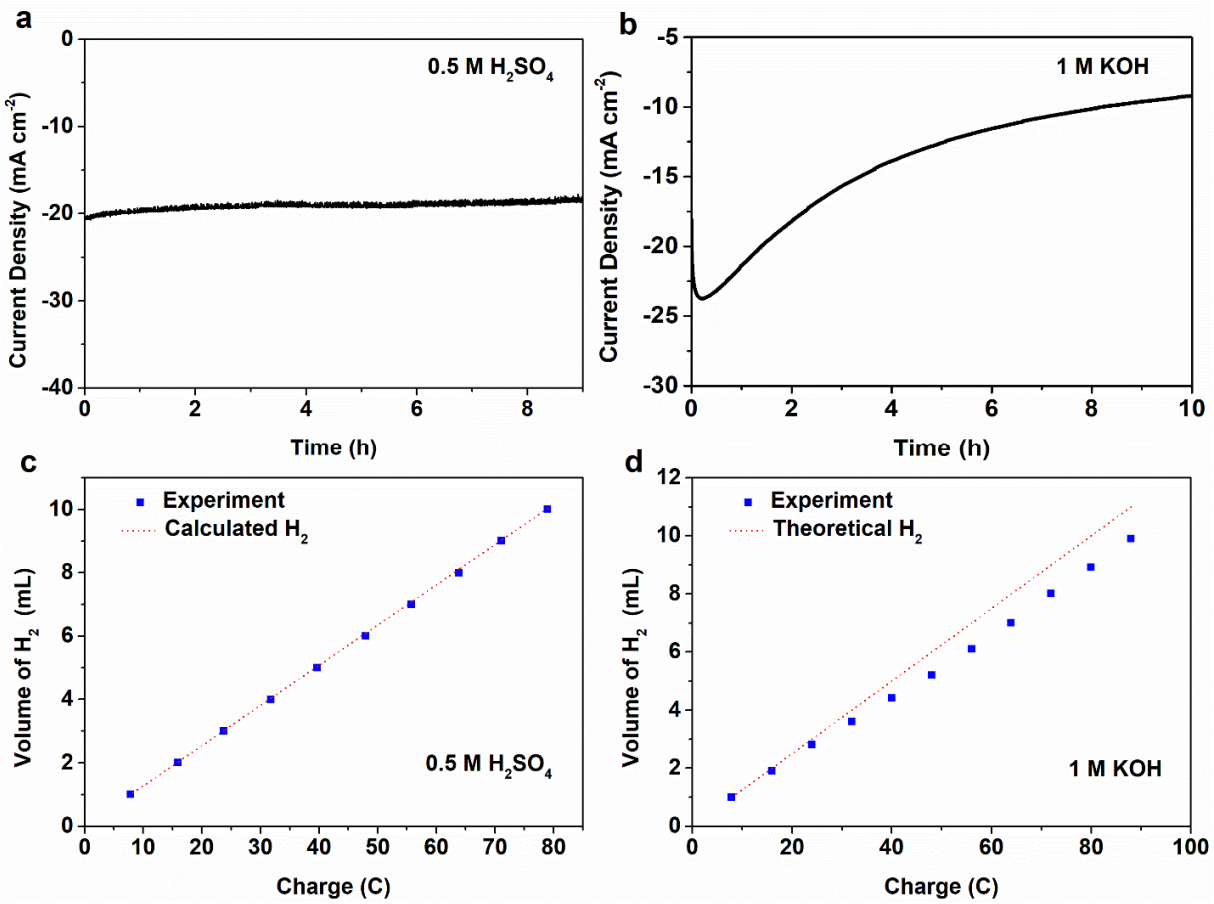

Figure 5. Stability test of FeP/Ti for HER in Ar-saturated (a) 0.5 M H_2SO_4 and (b) 1 M KOH. Amount of H_2 calculated according to the charge measured and experimental data of H_2 amount via water displacement method in (c) 0.5 M H_2SO_4 and (d) 1 M KOH.

Durability is another critical aspect of a catalyst for practical applications. Figure 5a and 5b show the current density of FeP/Ti in 0.5 M H_2SO_4 and 1 M KOH over a period of 10 hours. The FeP/Ti electrode displays a good stability in 0.5 M H_2SO_4, while the current drops continually with testing time in the 1 M KOH electrolyte. This indicates that FeP is not a stable catalyst for the HER in the basic environment. The Faradaic efficiency in acid solution is close to 100% (Figure 5c), while in alkaline solution it is below the 100% line (Figure 5d). Corrosion happens in the alkaline environment, which contributes the decreased current density with time. We found that HCl treatment could recover the activity (Figure S13), which indicates that the instability is caused by the corrosion product formed on the surface during the test, such as oxides. In order to further investigate the instability of FeP in alkaline environment, XPS was conducted.

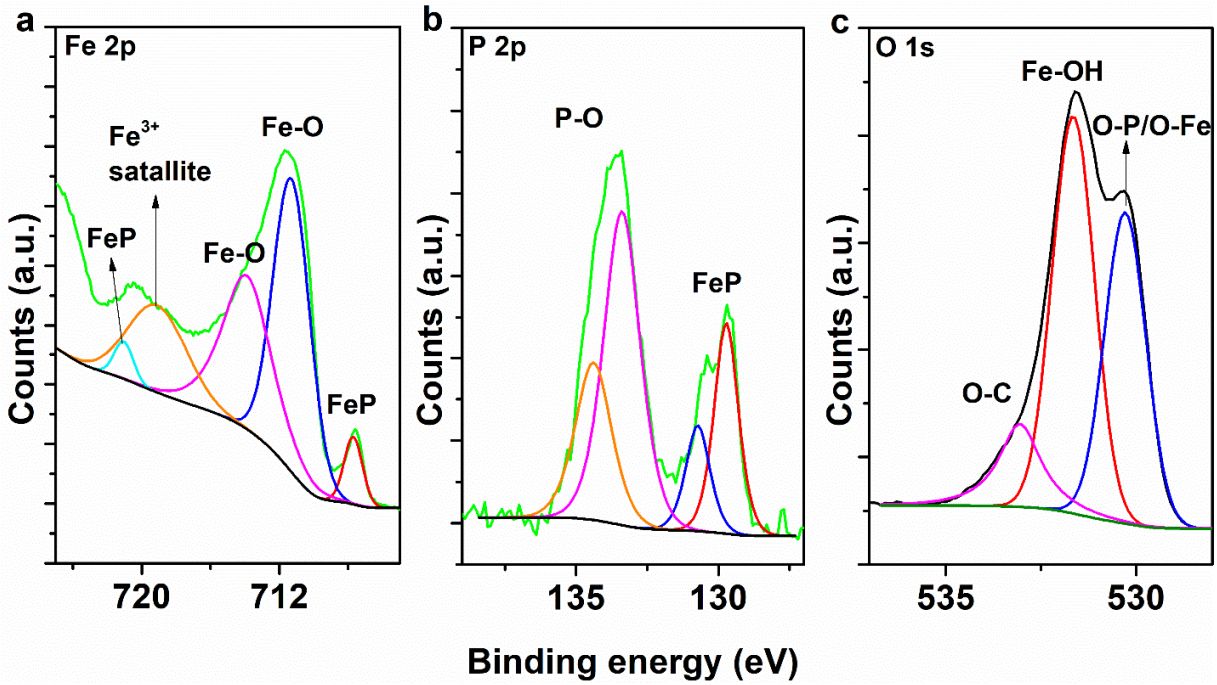

Figure 6. XPS spectra of (a) Fe 2p, (b) P 2p, and (c) O 1s for FeP after stability test in 1 M KOH for 10 hours.

The surface chemical states of Fe, P and O of the FeP with surface etching after long term stability test in 1 M KOH were analyzed to understand the reasons for instability (Figure 6). Compared with the sample after HCl etching, the obvious change observed on Fe 2p core level spectra is that more Fe-O bonds are present, and the typical satellite peaks of Fe^{3+} appear. This indicates that oxidation of iron happened on the surface. For P 2p core level spectra, P-O bond intensity increases as compared with the one after HCl etching. Also, another obvious change is reflected in the O 1s spectra. Two peaks at lower binding energy belonging to Fe-OH and Fe-O emerged after the stability test, which is very similar to the peaks of FeOOH (Figure S14).[35] Thus, we deduce the formation of FeOOH after the stability test in alkaline, and P is possibly oxidized into phosphate and dissolved in water. To confirm our speculation, we measured the PO_4^{3-} by ion chromatography. As expected, PO_4^{3-} was detected in the solution with concentration of 72.8 ppm. Hence, the formation of FeOOH on the surface due to the oxidation of FeP is the root cause for the instability.

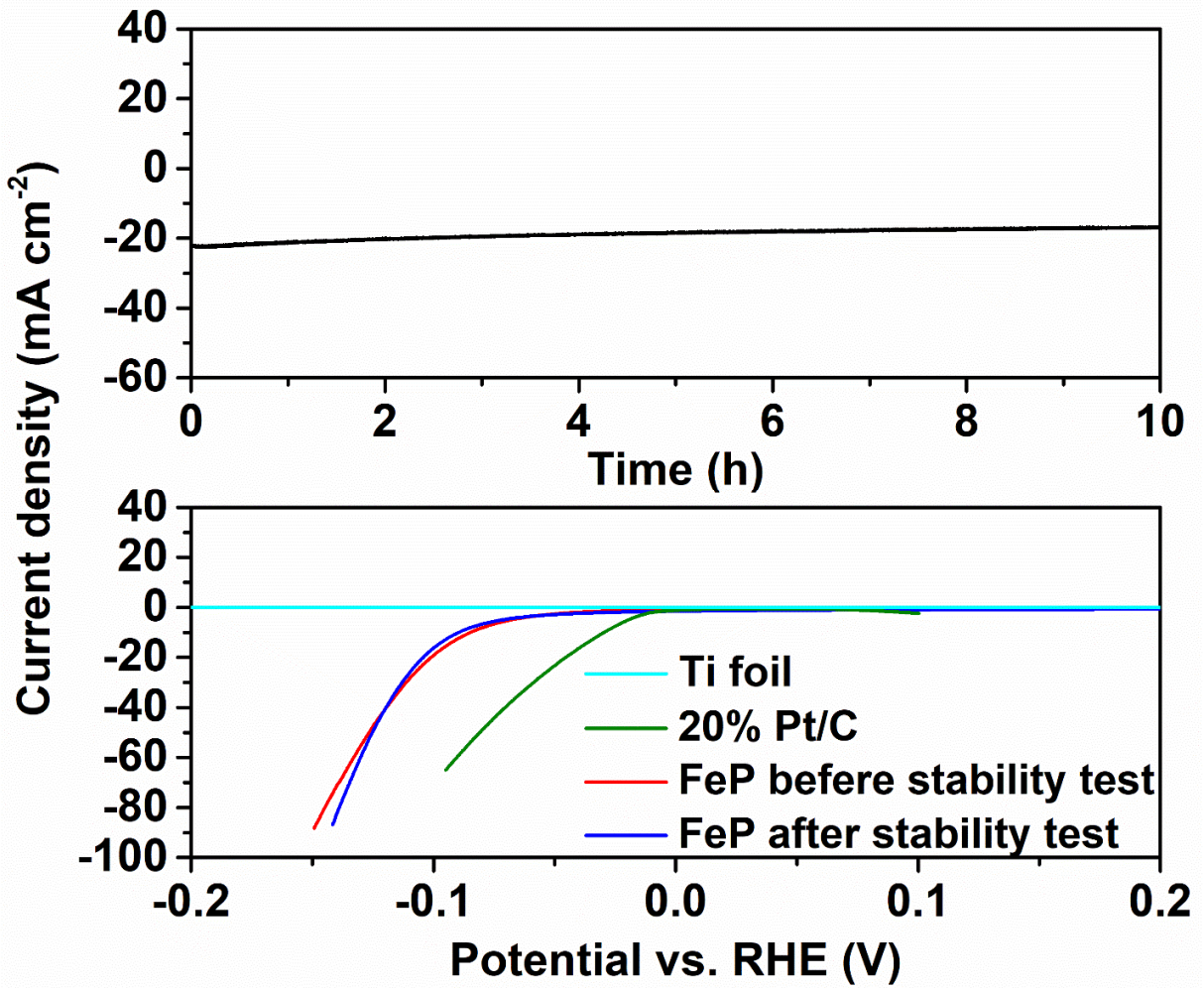

Figure 7. (a) Stability for the HER in 1 M KOH electrolyte with vacuum and Ar purge for several times with Ar bubbling for 1h. (b) The comparison of the HER performance of FeP in 1 M KOH electrolyte before and after stability test. HER performance of commercial 20% Pt/C and substrate Ti foil is also shown for comparison. The one after the stability test was carried out after 5 min Ar flow to carry the generated H_2 out of the closed reactor chamber.

To better understand the instability at molecular levels, theoretical calculations of the possible reactions in alkaline solution were considered (Table S6). We found that the instability of FeP was due to the presence of O_2. In other words, it can be stable in alkaline solution without the presence of O_2. To verify the calculated results, The FeP/Ti with surface HCl etching was used for the stability test under O_2 bubbling. The current dropped dramatically in 1 hour in the 1 M KOH electrolyte (Figure S15). We also soaked the FeP/Ti in 1 M KOH for 12 h without any applied bias. Before the soaking, air was bubbled in the solution for 10 min. We found that the color changed from black to yellow after soaking in 1 M KOH for 12 h. XRD confirmed that the diffraction peaks ascribed to FeP phase disappeared after the soaking (Figure S16). The yellow film on Ti foil is

FeOOH. Hence, O_2 is causing the oxidation of FeP and consequently the instability. It is noted that such oxidation is a chemical reaction, which occurs in the presence of O_2 in alkaline solution. Thus, even when FeP is used as a cathode electrode for reduction reaction, the oxidation reaction can still happen.

To improve the stability after identifying the root source, we conducted the test again in a sealed reactor. Before the test, Ar was purged into the reactor chamber for several times, and continuous Ar bubbling into the solution was carried out for 1 h before the test to minimize the oxygen content in solution. As expected, good stability was observed by removal of oxygen (Figure 7a). Although there was still a slight decrease in current after 10 h, the HER performance recovers to the initial level after we stopped the test for 5 minutes (Figure 7b). This means that the slight decrease was due to the accumulation of hydrogen gas inside the sealed reactor, which has hindered the forward reaction. After we carried away the accumulated H_2 by Ar flow, the performance could be fully recovered. For comparison, commercial 20%Pt/C was employed to fabricate electrode for HER according to previous report.[31] In addition, the HER activity of the FeP/Ti electrode in a neutral electrolyte was also measured and found unfavorable (Figure S17).

4. Conclusion

Nanosheet structured FeP grown on Ti foil has been synthesized as an HER electrocatalyst. The native oxide layer has been found on the surface of FeP nanosheet, which hinders the HER performance. Surface treatment in concentrated acid to remove the oxide layer can significantly improve the HER performance. After etching, the overpotentials in the acidic electrolyte (0.5M H_2SO_4) are 79 and 95 mV at 10 and 20 mA cm^{-2}, respectively. In the alkaline environment (1M KOH), the improvement is more significant: the overpotentials are reduced to 95 and 102 mV at 10 and 20 mA cm^{-2}, respectively. Such a good performance in alkaline electrolyte using FeP catalyst without any doping or modification has not been reported before. Theoretical calculation finds that surface O bond replacing P will decrease the activity of Fe sites compared with P sites. Oxygen is also the root source for the instability of FeP in the alkaline solution. Combining the experimental and theoretical calculation, it is found that the reaction with O_2 forming FeOOH on the surface has caused a higher overpotential required for the HER. On the basis of the analysis, we could achieve good stability in alkaline solution by conducting the test in a sealed reaction with the prior purge of Ar to remove the O_2 in solution.

Acknowledgement

Financial support from following is gratefully acknowledged: Ministry of Education (RG15/16, RG16/18) of Singapore government, Singapore National Research Foundation through the Singapore-Berkeley Initiative for Sustainable Energy (SINBERISE) CREATE Programme, National Natural Science Foundation of China (No. 21676216)

References

[1] P. Jiang, Q. Liu, Y. Liang, J. Tian, A.M. Asiri, X. Sun, Angew. Chem., 126 (2014) 13069-13073.
[2] Y. Li, H. Wang, L. Xie, Y. Liang, G. Hong, H. Dai, J. Am. Chem. Soc., 133 (2011) 7296-7299.
[3] J. Hu, S. Zheng, X. Zhao, X. Yao and Z. Chen, J. Mater. Chem. A, 2018, 6, 7827-783

[4] J.A. Turner, Science, 305 (2004) 972-974.
[5] G. Jia, W. Zhang, G. Fan, Z. Li, D. Fu, W. Hao, C. Yuan, Z. Zou, Angew. Chem. Int. Ed., 56 (2017) 13781-13785.
[6] Z. Xu, W. Li, X. Wang, B. Wang, Z. Shi, C. Dong, S. Yan, Z. Zou, ACS Appl. Mater. Inter., 10 (2018) 30357-30366.
[7] C. Y. Son, I. H. Kwak, Y. R. Lim and J. Park, Chem. Commun., 2016, **52**, 2819-2822.
[8] J. Tian, J. Chen, J. Liu, Q. Tian, P. Chen, Nano Energy, 48 (2018) 284-291.
[9] D.-H. Ha, B. Han, M. Risch, L. Giordano, K.P. Yao, P. Karayaylali, Y. Shao-Horn, Nano Energy, 29 (2016) 37-45.
[10] J. Chen, J. Liu, J.-Q. Xie, H. Ye, X.-Z. Fu, R. Sun, C.-P. Wong, Nano Energy, 56 (2019) 225-233.
[11] C.Y. Son, I.H. Kwak, Y.R. Lim, J. Park, Chem. Commun., 52 (2016) 2819-2822.
[12] Z. Liu, Z. Gao, F. Luo, S. Yuan, K. Wang, N. Li, X. Li, ChemCatChem, 10 (2018) 3441-3446.
[13] P. Xiao, W. Chen, X. Wang, Adv. Energy Mater., 5 (2015) 1500985.
[14] Y. Xu, R. Wu, J. Zhang, Y. Shi, B. Zhang, Chem. Commun., 49 (2013) 6656-6658.
[15] Y. Liang, Q. Liu, A.M. Asiri, X. Sun, Y. Luo, ACS Catal., 4 (2014) 4065-4069.
[16] Y. Yan, L. Thia, B.Y. Xia, X. Ge, Z. Liu, A. Fisher, X. Wang, Adv. Sci., 2 (2015) 1500120.
[17] Y. Yan, B. Zhao, S.C. Yi, X. Wang, J. Mater. Chem. A, 4 (2016) 13005-13010.
[18] D. Li, Q. Liao, B. Ren, Q. Jin, H. Cui, C. Wang, J. Mater. Chem. A, 5 (2017) 11301-11308.
[19] H. Du, S. Gu, R. Liu, C.M. Li, Int. J. Hydrogen Energy, 40 (2015) 14272-14278.
[20] Y. Yan, B.Y. Xia, X. Ge, Z. Liu, A. Fisher, X. Wang, Chem. Eur. J., 21 (2015) 18062-18067.
[21] J. Tian, Q. Liu, Y. Liang, Z. Xing, A.M. Asiri, X. Sun, ACS Appl. Mater. Inter., 6 (2014) 20579-20584.
[22] Z. Zhang, B. Lu, J. Hao, W. Yang, J. Tang, Chem. Commun., 50 (2014) 11554-11557.
[23] X. Guo, Z. Feng, Z. Lv, Y. Bu, Q. Liu, L. Zhao, C. Hao, G. Li, Q. Lei, ChemElectroChem, 4 (2017) 2052-2058.
[24] X. Yang, A.-Y. Lu, Y. Zhu, S. Min, M.N. Hedhili, Y. Han, K.-W. Huang, L.-J. Li, Nanoscale, 7 (2015) 10974-10981.
[25] X.F. Lu, L. Yu, X.W.D. Lou, Sci. adv., 5 (2019) 6009.
[26] X. Peng, A.M. Qasim, W. Jin, L. Wang, L. Hu, Y. Miao, W. Li, Y. Li, Z. Liu, K. Huo, Nano Energy, 53 (2018) 66-73.
[27] F. Yu, H. Zhou, Y. Huang, J. Sun, F. Qin, J. Bao, W.A. Goddard, S. Chen, Z. Ren, Nat. Commun., 9 (2018) 2551.
[28] F. Wang, X. Yang, B. Dong, X. Yu, H. Xue, L. Feng, Electrochem. Commun., 92 (2018) 33-38.
[29] N.K.A. Venugopal, S. Yin, Y. Li, H. Xue, Y. Xu, X. Li, H. Wang, L. Wang, Chem. Asian J., 13 (2018) 679-685.
[30] S. Jiao, L. Xu, K. Hu, J. Li, S. Gao, D. Xu, J. Phys. Chem. C, 114 (2009) 269-273.
[31] X.-D. Wang, Y.-F. Xu, H.-S. Rao, W.-J. Xu, H.-Y. Chen, W.-X. Zhang, D.-B. Kuang, C.-Y. Su, Energy Environ. Sci., 9 (2016) 1468-1475.
[32] Y. Wang, P.M. Sherwood, Surf. Sci. Spectra, 9 (2002) 99-105.
[33] R. Liu, S. Gu, H. Du, C.M. Li, J. Mater. Chem. A, 2 (2014) 17263-17267.
[34] D.Y. Chung, S.W. Jun, G. Yoon, H. Kim, J.M. Yoo, K.-S. Lee, T. Kim, H. Shin, A.K. Sinha, S.G. Kwon, J. Am. Chem. Soc., 139 (2017) 6669-6674.
[35] G. Park, Y.-I. Kim, Y.H. Kim, M. Park, K.Y. Jang, H. Song, K.M. Nam, Nanoscale, 9 (2017) 4751-4758.